Hemi-Fontan and bidirectional Glenn operations result in flow-mediated viscous energy loss at the time of stage II palliation

Michal Schäfer, MD, PhD,[a] Michael V. Di Maria, MD,[b] James Jaggers, MD,[a] Matthew L. Stone, MD, PhD,[a] David N. Campbell, MD,[a] D. Dunbar Ivy, MD,[b] and Max B. Mitchell, MD[a]

ABSTRACT

Background: Superior cavopulmonary connection (SCPC) for stage II palliation of hypoplastic left heart syndrome (HLHS) is achieved most frequently by either a bidirectional Glenn (BDG) or hemi-Fontan (HF) operation. The comparison of flow hemodynamic efficiency at the region of surgical reconstruction and in proximal pulmonary arteries has been evaluated primarily using computational modeling techniques with conflicting reports. The purpose of this descriptive study was to compare flow hemodynamics following stage II (BDG vs HF) using 4-dimensional flow magnetic resonance imaging (4D-Flow MRI) with particular focus on flow-mediated viscous energy loss (E_L') under matched hemodynamic conditions.

Methods: Patients with hypoplastic left heart syndrome (HLHS) who underwent either HF or BDG as part of stage II palliation underwent pre-Fontan 4D-Flow MRI. Patients were matched by the pulmonary vascular resistance index, net superior vena cava (SVC) flow, right pulmonary artery (RPA) and left pulmonary artery (LPA) size, and age. Maximum E_L' throughout the cardiac cycle was calculated along the SVC-RPA and SVC-LPA tracts.

Results: Eight patients who underwent HF as part of their stage II single ventricle palliation were matched with 8 patients who underwent BDG. There were no differences between the 2 groups in median volumetric indices, including end-diastolic volume ($P = .278$) and end-systolic volume ($P = .213$). Moreover, no differences were observed in ejection fraction ($P = .091$) and cardiac index ($P = .324$). There also were no differences in peak E_L' measured along the SVC-RPA tract (median, 0.05 mW for HF vs 0.04 mW for BDG; $P = .365$) or along the SVC-LPA tract (median, 0.05 mW vs 0.04 mW; $P = .741$).

Conclusions: The second stage of surgical palliation of HLHS using either HF or BDG results in similar flow-mediated viscous energy loss throughout the SCPC junction. 4D-Flow MRI and computational methods should be applied together to investigate flow hemodynamic patterns throughout the Fontan palliation and overall efficiency of the Fontan circuit. (JTCVS Open 2023;16:836-43)

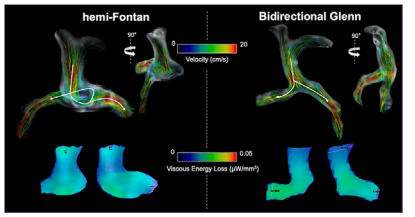

Comparison of HF and BDG flow hemodynamic patterns.

CENTRAL MESSAGE

The second stage of surgical palliation of HLHS using either HF or BDG results in similar flow-mediated viscous energy loss throughout the SCPC junction.

PERSPECTIVE

Four-dimensional flow (4D-Flow) MRI results complement previous computational results suggesting minimal differences in mechanical fluid dissipating energy loss, particularly in the context of the entire pulmonary circuit. 4D-Flow MRI and computational methods should be applied together to investigate flow hemodynamic patterns throughout the Fontan palliation procedure.

Stage II surgical palliation for hypoplastic left heart syndrome (HLHS) by a superior cavopulmonary connection results in nonpulsatile flow from the superior vena cava (SVC) to the pulmonary arteries (PAs) independent of ventricular support. Therefore, the aim of surgical reconstruction is to yield a system with minimal pressure and energy loss in the proximal PAs.[1] Superior cavopulmonary connection (SCPC) for stage II palliation is achieved most frequently via either the bidirectional Glenn (BDG) or hemi-Fontan (HF) operation. Whereas the BDG operation creates a communication between the SVC and undivided PAs, the HF procedure augments the PA without dividing the SVC and excludes flow from the inferior vena cava by means of a temporary atrial patch.[2,3] The majority of studies

From the [a]Division of Cardiothoracic Surgery, University of Colorado Denver, Anschutz Medical Campus, Aurora, Colo; and [b]Division of Pediatric Cardiology, Children's Hospital Colorado, University of Colorado Denver, Anschutz Medical Campus, Aurora, Colo.

Read at the 49th Annual Meeting of the Western Thoracic Surgical Association, Coeur d'Alene, Idaho, June 26-29, 2013

Received for publication June 20, 2023; revisions received Aug 24, 2023; accepted for publication Sept 8, 2023; available ahead of print Oct 24, 2023.

Address for reprints: Michal Schäfer, MD, PhD, Heart Institute, Children's Hospital Colorado, 13123 E 16th Ave, Aurora, CO 80045-2560 (E-mail: michal.schafer@cuanschutz.edu).

2666-2736

https://doi.org/10.1016/j.xjon.2023.09.030

Abbreviations and Acronyms

4D-flow MRI = four-dimensional flow magnetic resonance imaging
BDG = bi-directional Glenn
E_L' = viscous energy loss
HF = hemi-Fontan
HLHS = hypoplastic left heart syndrome
SCPC = superior cavopulmonary connection
SVC = superior vena cava

evaluating pulmonary circulation in patients with single ventricle physiology have focused on the hemodynamic state after completed palliation[4,5]; however, a direct comparison of the flow hemodynamic state between the operative techniques at intermediate stage II using in vivo flow imaging has not yet been done.

The comparison of flow hemodynamic efficiency at the region of surgical reconstruction and in proximal PAs has been evaluated primarily using computational modeling.[6] Computational studies have reported conflicting results on fluid energy dissipation loss through the SCPC and proximal PAs, likely related to different methodologic approaches.[6-8] In contrast to computational methods, 4D-Flow MRI measures velocity directly and does not rely on assumptions about physiologic boundary conditions, such as vascular compliance and resistance; however, it lacks spatiotemporal resolution.[9] Lately, interrogation of the Fontan circulation using 4D-Flow MRI flow-mediated viscous energy loss (E_L') has proven feasible.[10-12] Unlike hydraulic or mechanical fluid energy loss, E_L' is a form of frictional energy loss due to viscous interaction within the fluid domain and indirectly measures the amount of flow inefficiency due to secondary flow characteristics, such as vortices or helices.[13]

Thus, the purpose of this descriptive study was to compare flow hemodynamics following stage II (BDG vs HF) using 4D-Flow MRI, with a particular focus on flow-mediated E_L' under matched hemodynamic conditions. We present the results of this series to propose an additional flow hemodynamic parameter to complement previous computational studies concerning the interstage phase of HF palliation.

METHODS

This descriptive study was a part of larger prospective study investigating flow hemodynamic conditions in children with congenital heart disease using cardiac MRI and 4D-Flow MRI approved by the Colorado Multi-Institutional Review Board with a waiver of written consent (19-1420; date of approval, June 20, 2019). Cardiac MRI including 4D-Flow MRI is currently part of standard pre-Fontan evaluation in addition to echocardiographic and catheterization evaluations at our institution. All the patients in this series had a history of HLHS palliated initially by the Norwood procedure and followed by either HF or BDG. Patients were pairwise matched by physiologic, geometric, and demographic parameters, including pulmonary vascular resistance index, net SVC flow, branch PA size, and age at MRI acquisition. Patients with a significant stenotic lesion treated with stent or balloon angioplasty were excluded. A waiver of informed consent in the study population was approved, and all procedures were performed in accordance with the principles outlined in the Declaration of Helsinki.

Cardiac MRI Protocol

All patients underwent standardized cardiac magnetic resonance (CMR) evaluation following our previously described institutional protocol, with prescribed sequences customized for single ventricle evaluation.[14] A 3.0-T system (Ingenia; Philips Medical Systems) was used to acquire balanced steady-state free precession stacks of short-axis images covering the ventricles from base to apex. Long-axis and 4-chamber views were obtained in each subject, with plane orientations chosen to appreciate the atrioventricular valves and outflow tracts. Finally, trough plane views of the SCPC and proximal PAs were obtained.

The 4D-Flow MRI protocol was as described previously.[15] In brief, 4D-Flow MRI sequences were acquired in the sagittal plane with typical sequence parameters as follows: echo time, 2.4 to 2.6 msec; repetition time, 4.2 to 5.0 msec; flip angle, 10°; temporal resolution, 42 to 50 msec; field of view, 250 × 320 or 200 × 250 mm^2; 14 to 18 cardiac phases; voxel size, 2.0 to 2.4 × 2.0 to 2.4 × 2.2 to 2.6 mm^3; velocity encoding, 100 to 150 cm/s; and acquisition time, 10 to 15 minutes, depending on respiratory gating efficiency.

Viscous Energy Loss Calculation

Power loss refers to the mechanical fluid energy dissipation loss as blood is moved along the vasculature. This is determined primarily by the pressure differences, and this "hydraulic" power loss has been preferentially investigated in computational fluid dynamic studies. Under real-life conditions, there are also additional mechanical energy losses related to friction, which could be due to viscous (E_L') or turbulent energy losses. E_L' is inversely related to vessel radius and is the main cause of energy loss in stationary laminar flow, which closely resembles Fontan circulation. E_L' can be further increased if the flow through a vessel is not laminar/cohesive and creates secondary flow formations, such as vortices and helices.

Flow-mediated viscous energy loss, E_L', was calculated in each patient along the predefined vascular tracked, as proposed previously[16] (Figure 1). All postprocessing steps were done using a commercially available postprocessing platform (Circle CVI42; Circle Cardiovascular Imaging). Anatomic structures were identified from 4D-Flow MRI–derived magnetic resonance angiography, which served for subsequent structural segmentation. Segmented contours of the SVC, SCPC, and PAs served for the regional delineation and definition of the centerline along which E_L' was calculated. The first path included a segment from the SVC starting at the junction of the innominate veins and followed a centerline through the SCPC and approximately 2 cm to the right PA (RPA). The second path started at the same location at the innominate vein junction and followed a centerline to the left PA (LPA). Peak E_L' encountered throughout the cardiac cycle was recorded for each patient and adjusted for total centerline length. The determination of instantaneous viscous energy loss due to frictional forces was calculated per individual voxel within a predefined segmented region and yielded units of power loss in milliWatts (mW).

Statistical Analysis

This was primarily a descriptive study, and collected demographic and hemodynamic values are reported as mean ± standard deviation or median with corresponding interquartile range as dictated by the dataset distribu-

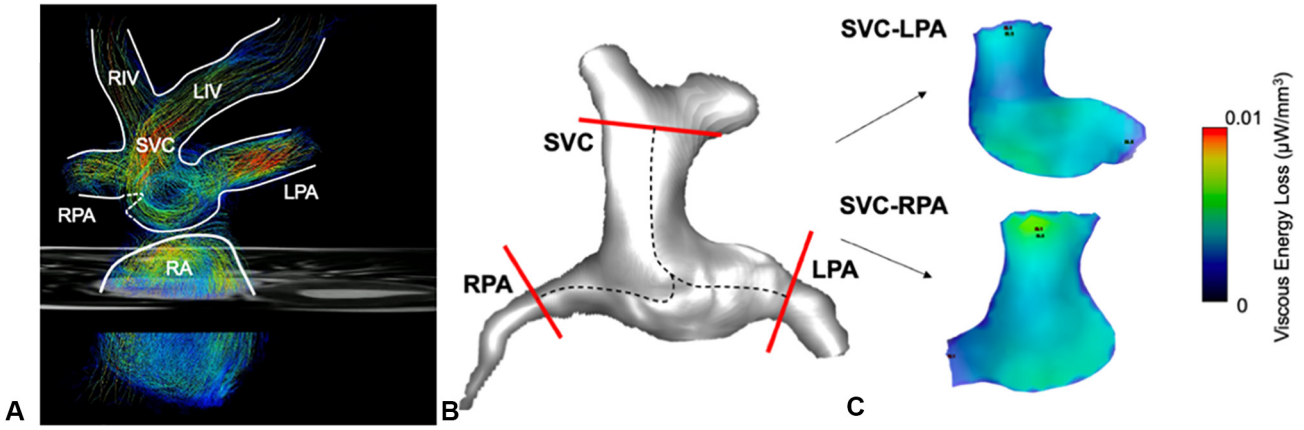

FIGURE 1. Post-processing workflow of the 4-dimensional flow magnetic resonance imaging (*4D-Flow MRI*) datasets. A, Qualitative flow visualization and inspection of generated pathlines was performed. B, 4D-Flow MRI derived angiography was used to segment the superior vena cava (*SVC*) and right pulmonary artery (*RPA*) and left pulmonary artery (*LPA*). C, Viscous energy loss was then calculated along the SVC-RPA and SVC-LPA tracts. *RIV*, Right innominate vein; *LIV*, left innominate vein; *RA*, right artery.

tion. Pairwise matching was based on parameters directly influencing E_L', including flow rate (net flow through the SVC) and PA diameters, as well as physiologic and demographic parameters including pulmonary vascular resistance index, age at MRI acquisition, and age at stage II operation. Patients were matched 1:1 based on propensity score matching. The probability of undergoing HF versus BDG was calculated by a multivariable logistic regression model that contained pulmonary vascular resistance index, net SVC flow, size of branch PAs, and age at MRI acquisition. Comparative analyses of flow hemodynamic parameters between HF patients and BDG patients were performed using the paired Wilcoxon rank-sum test. All statistical analyses and data presentation were performed with Prism version 9.5.1 (GraphPad Software), and Gardner-Altman figures were generated using estimation plots.[17] All tests were 2-sided, and significance was based on an α level of $\leq$0.05.

RESULTS

In this study, 8 patients who underwent HF as part of their stage II single ventricle palliation were matched with 8 patients who underwent BDG. Patient demographics and hemodynamic characteristics are reported in Table 1. Specific diagnoses included HLHS with aortic atresia/mitral stenosis (n = 6), aortic atresia/mitral atresia (n = 4), and aortic stenosis/mitral stenosis (n = 6). All patients underwent the Norwood procedure as part of their initial palliation with a right ventricle-to-PA shunt (n = 9) or modified Blalock-Taussig shunt (n = 7). The median age at the time of stage II operation was 5 months in both the HF and BDG patient groups, and the median age at the time of current 4D-Flow MRI scan was 2.5 years in both groups. There was no between-group difference in pre-Fontan pulmonary vascular resistance index (1.9 WU for HF vs 2.1 WU for BDG; P = .641). No differences were observed in median net SVC flow or branch PA diameters and their respective z-scores. No patient had worse than mild-to-moderate tricuspid regurgitation on same-day echocardiography. Eventually, all patients successfully underwent the

TABLE 1. Patient characteristics and hemodynamic parameters

Variable	HF (N = 8)	BDG (N = 8)	*P* value
Age at 4D-Flow MRI, y, median (IQR)	2.5 (2.0-3.1)	2.5 (2.0-3.0)	.641
Female sex, n (%)	3 (38)	3 (38)	—
BSA, m^2, median (IQR)	0.61 (0.56-0.63)	0.59 (0.56-0.63)	.766
Age at stage II, mo, median (IQR)	5 (4-6)	5 (4-6)	.925
SVC net flow, mL, median (IQR)	11.5 (9.9-12.3)	9.9 (8.4-11.5)	.209
PVRi, WU, median (IQR)	1.9 (1.6-2.2)	2.1 (1.6-3.0)	.641
RPA diameter, cm, median (IQR)	1.0 (0.8-1.1)	1.0 (0.9-1.1)	.661
RPA z-score, median (IQR)	0.4 (−0.7 to 0.9)	0.5 (−0.6 to 0.7)	.516
LPA diameter, cm, median (IQR)	1.0 (0.7-1.1)	0.8 (0.6-0.9)	.492
LPA z-score, median (IQR)	1.0 (−0.8 to 1.8)	−0.2 (−1.0 to 0.3)	.357

Reported *P* values are from the paired Wilcoxon matched-pair rank-sum test. *HF*, Hemi-Fontan; *BDG*, bidirectional Glenn; *4D-Flow MRI*, 4-dimensional flow magnetic resonance imaging; *IQR*, interquartile range; *BSA*, body surface area; *SVC*, superior vena cava; *PVRi*, pulmonary vascular resistance index; *WU*, Woods unit; *RPA*, right pulmonary artery; *LPA*, left pulmonary artery.

TABLE 2. 4D-Flow MRI hemodynamics

Parameter	HF (N = 8)	BDG (N = 8)	*P* value
End-diastolic volume index, L/m^2, median (IQR)	130 (11-160)	105 (103-111)	.278
End-systolic volume index, L/m^2, median (IQR)	71 (54-83)	50 (45-56)	.213
Stroke volume index, L/m^2, median (IQR)	61 (56-62)	53 (50-63)	.954
Ejection fraction, %, median (IQR)	48 (42-51)	50 (48-56)	.091
Cardiac index, L/min/m^2, median (IQR)	4.7 (4.2-5.0)	5.5 (5.1-6.1)	.324
AP collateral flow, %, median (IQR)	34 (29-38)	46 (34-50)	.275
SVC-RPA E_L', mW, median (IQR)	0.05 (0.03-0.07)	0.04 (0.03-0.06)	.365
SVC-LPA E_L', mW, median (IQR)	0.05 (0.03-0.07)	0.04 (0.03-0.10)	.741

Reported *P* values represent paired Wilcoxon matched pair rank tests. *HF*, Hemi-Fontan; *BDG*, bidirectional Glenn; *IQR*, interquartile range; *AP*, aortopulmonary; *SVC*, superior vena cava; *RPA*, right pulmonary artery; *LPA*, left pulmonary artery; E_L', viscous energy loss; *4D-Flow MRI*, 4-dimensional flow magnetic resonance imaging.

HF procedure without major complications necessitating further reoperation.

Cardiac 4D-Flow MRI hemodynamics are summarized in Table 2. There were no differences in median volumetric indices, including end-diastolic volume (median, 130 mL/m^2 for HF vs 105 mL/m^2 for BDG; $P = .278$) and end-systolic volumes (median, 71 mL/m^2 vs 50 mL/m^2, respectively; $P = .213$). In addition, no differences were observed in ejection fraction (median, 48% for HF vs 50% for BDG; $P = .091$), cardiac index (median, 4.7 L/min/m^2 vs 5.5 L/min/m^2; $P = .324$), or aortopulmonary collateral flow burden (median, 34% vs 46%; $P = .275$).

A comparison of the 4D-Flow MRI-derived E_L' is delineated in Table 2 and graphically depicted by Gardner-Altman plots in Figure 2. There were no differences in peak E_L' measured along the SVC-RPA tract (median, 0.05 mW for HF vs 0.04 mW for BDG; $P = .365$) and the SVC-LPA tract (median, 0.05 mW vs 0.04 mW; $P = .741$). Qualitatively, flow patterns were distinctively different between the HF and BDG groups (Figure 3). In patients with the HF configuration, flow through the SVC is projected to the respective PAs already at the level of floor of the patch dividing the SVC. The portion of the flow directed to the RPA typically creates a secondary flow formation in a helical form, as was observed in 5 of the 8 (63%) HF patients. This flow pattern appears to result from an incoming flow trajectory when pathlines collide with the posterior wall of the PA and rebounce again on the posterior aspect of the SVC or PA, giving a rise to a helical formation (Figure 4). This helical flow pattern was absent in the LPA in all HF patients.

In contrast to HF patients, in all BDG patients the BDG configuration resulted in a cohesive uniform flow without any secondary flow formations proximal or distal to the SCPC region. The flow through the SVC typically splits directly at the level of the SVC-PA junction, with further redirection dictated by the geometric orientation of the PAs without any vortical or helical formations.

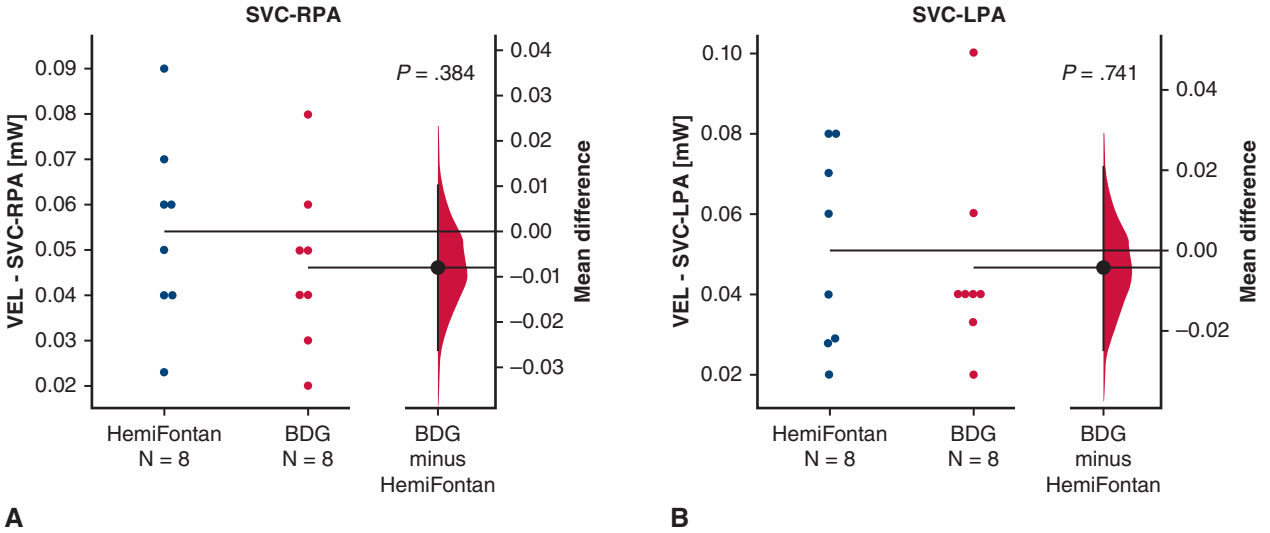

FIGURE 2. Graphical depiction of the comparative analysis of viscous energy loss between the hemi-Fontan (*HF*) and bidirectional Glenn (*BDG*) techniques along the superior vena cava (*SVC*)–right pulmonary artery (*RPA*) (A) and SVC–left pulmonary artery (*LPA*) (B) paths. *VEL*, viscous energy loss.

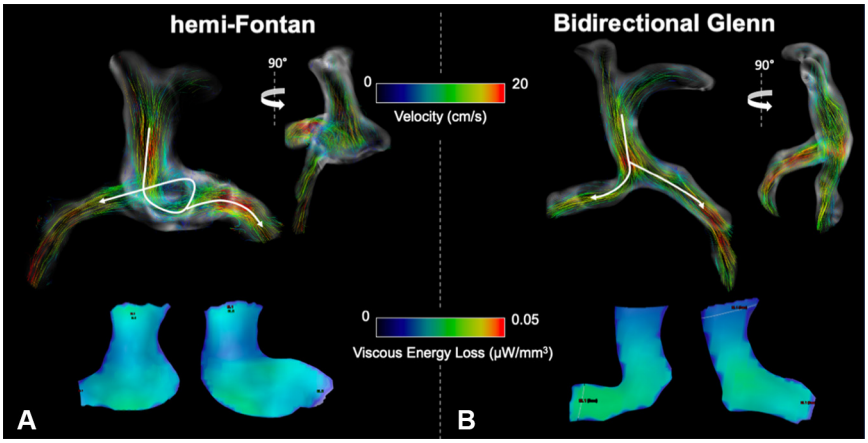

FIGURE 3. Representative comparison of the hemi-Fontan (*HF*) (A) and bidirectional Glenn (*BDG*) (B) 4-dimensional flow magnetic resonance imaging (*4D-Flow MRI*) cases and corresponding viscous energy loss heat maps along the superior vena cava to branch pulmonary arteries. *White arrows* indicate a predominant pathline trajectory to the respective branch pulmonary arteries. A minor helical formation can be seen in the lateral view of the right pulmonary artery of the patient who underwent the HF procedure. This helix was noted in 5 of 8 HF cases and was absent in all BDG cases.

DISCUSSION

In this descriptive study, we report comprehensive qualitative and quantitative flow hemodynamic indices in patients who underwent either HF or BDG as the second stage of their surgical palliation for HLHS. The primary findings of this report can be summarized as follows: (1) there were no quantitative differences between the 2 procedures in flow patterns, as evaluated by E_L' with minor qualitative flow differences in RPA; and (2) there were no differences in standard pre-Fontan cardiac MRI hemodynamics. These findings are further highlighted by similar physiologic and geometric conditions in the 2 patient groups. Our results supplement findings from previous computational studies with direct in vivo 4D-Flow MRI measurements and suggest the feasibility of flow hemodynamic mapping prior to completion of Fontan palliation.

To the best of our knowledge, all previous studies comparing flow hemodynamic efficiency of the SCPC using either the HF or BDG surgical approach have been accomplished using computational simulations with variable outcomes.[6-8,18] Variable study designs and approaches defining the geometric boundary conditions using different imaging modalities with physiologic inputs derived from catheterization or phase-contrast MRI are a likely cause of the minor discrepancies in observed results. The earliest comparative study using computational fluid dynamics by Bove and colleagues[6] investigated hydraulic power loss. The authors observed no differences at stage II but reported higher energy losses in patients who underwent BDG after completion of Fontan procedures. A subsequent study by Pekkan and colleagues[8] found that the BDG connection is hemodynamically more efficient compared to HF using stereolithographic models of patient-specific anatomies in combination with phase-contrast MRI data serving as the flow input. A recent study by Kung and colleagues[7] applied multiscale modeling approach using the same patient preoperative anatomies and virtually superimposed either the HF or the BDG template on the final hemodynamic system. The authors observed highly variable energy losses at the level of the SCPC junction between the 2 techniques, with slightly worse hydraulic energy loss in some HF patients; critically, they also reported that the local power losses have a negligible effect on the entire pulmonary circulation, and that final physiologic and hemodynamic outcomes were similar in the 2 groups.

It is important to consider measured flow-mediated energy loss in the context of the entire pulmonary circuit and single ventricular power. Most studies have reported local energy loss in the range of 0.1 to 3.5 mW. Studies modeling HF surgical configuration showed that total mechanical power loss across the entire pulmonary bed can exceed 15 mW, and consequently, local flow-mediated energy dissipation was calculated to represent 1% to 16% of the overall energy loss and <2% of ventricular power loss.[7,19] However, this energy loss can be more severe in the setting of proximal pulmonary arterial stenosis and might be more profound during exercise.[20] In patients with the BDG configuration, a highly uneven flow ratio to the branch PAs has been shown to increase flow energy loss, with the minimal energy loss achieved at near-normal physiologic 55% split flow to the RPA.[21] Additional consideration should be given to the shear-dependent blood viscosity, otherwise known as non-Newtonian behavior, describing a nonlinear relationship between shear stress and shear strain at low-velocity venous flow conditions. A study by Cheng and colleagues[22] showed that considering this physiologic property significantly alters flow hemodynamic outcomes, including power loss, pulmonary flow

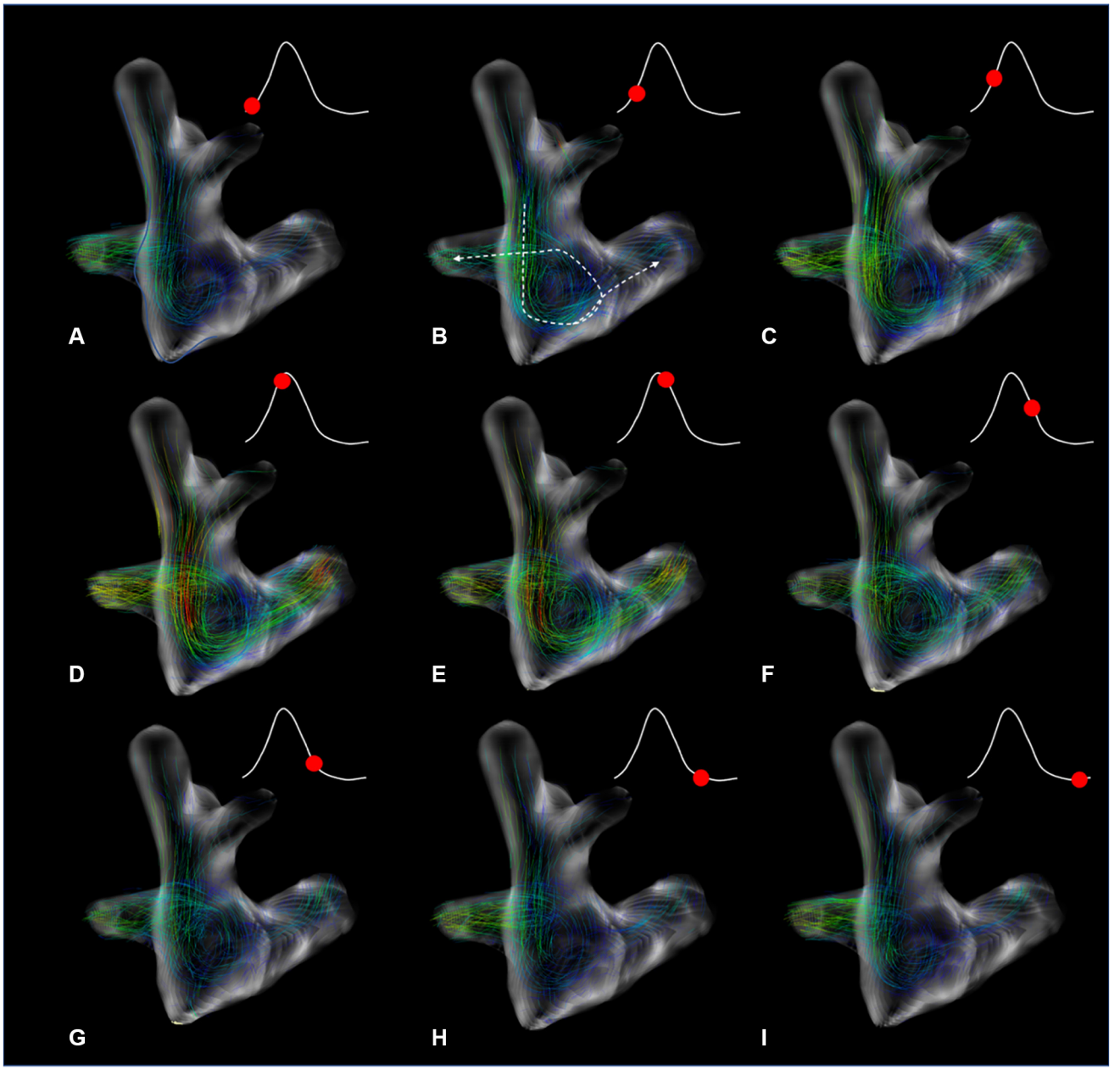

FIGURE 4. A-I, Temporal evolution of flow in the representative hemi-Fontan configuration throughout the cardiac cycle. No secondary flow formations were observed in the area of the cavoatrial junction, but a small helix in the right pulmonary artery can be appreciated in mid-systolic phase.

distribution, shear stress, and caval flow mixing in Fontan circulation, yet this property is often omitted in computational studies.

Our data show that flow-mediated viscous energy loss, E_L', in the pre-Fontan stage ranges from 0.02 to 0.10 mW, which is approximately one-third lower than values reported in studies evaluating the completed total cavopulmonary anastomosis.[12,23] Based on our results and on previously discussed computational studies, we believe that E_L' and the quality of flow formations have only minor roles in the overall mechanical energy loss in the pulmonary circuit, particularly in circuits with significant stenoses. However, E_L' represents only mechanical energy loss due to frictional losses, and thus the overall hydraulic energy loss is underestimated. Furthermore, although 4D-Flow MRI–derived E_L' measurements are considered reliable in comparative studies,[24] they typically underestimate the true E_L', as shown by computational studies.[11] Qualitatively observed helical flow through the RPA in HF did not significantly increase E_L'. We speculate that this is due primarily to the low-velocity flow system and relatively short distance along which the E_L' was measured. In addition, the role of helical flow through large vessels merits further exploration, as higher helicity has been previously associated

with better hemodynamic outcomes in patients with pulmonary hypertension.[25,26] Future studies using 4D-Flow MRI–estimated E_L' should be evaluated in the context of stress exercise using MRI-compatible devices to appreciate the energy loss in the context of higher myocardial workload.

Limitations

This early-stage descriptive study considered only patients without significant stenoses and with favorable pre-Fontan stage hemodynamics, resulting in a significant patient selection bias. Furthermore, this was only a single-center study reflective of surgical techniques at our institution. At this time, we also did not have post-Fontan stage flow hemodynamic parameters for a final outcome comparison of the 2 techniques. Additional limitations are pertinent primarily to the 4D-Flow MRI technique, including limited spatiotemporal resolution and the inability to study flow hemodynamic patterns in patients with implanted stents. We believe that multimodality studies involving both 4D-Flow MRI and computational fluid dynamics would be highly beneficial for investigating flow hemodynamic patterns and their overall role during the interstage phase of the Fontan palliation and in long-term clinical outcomes.

CONCLUSIONS

The second stage of surgical palliation of HLHS using either HF or BDG results in similar flow-mediated viscous energy loss throughout the SCPC junction. Our 4D-Flow MRI results complement previous computational results suggesting minimal differences in mechanical fluid dissipating energy loss, particularly in the context of the entire pulmonary circuit. 4D-Flow MRI and computational methods should be applied together to investigate flow hemodynamic patterns throughout the Fontan palliation and to investigate the role of flow-mediated energy loss in predicting clinical outcomes and overall efficiency of the Fontan circuit.

Conflict of Interest Statement

The authors reported no conflicts of interest.

The *Journal* policy requires editors and reviewers to disclose conflicts of interest and to decline handling or reviewing manuscripts for which they may have a conflict of interest. The editors and reviewers of this article have no conflicts of interest.

References

1. Rychik J, Atz AM, Celermajer DS, Deal BJ, Gatzoulis MA, Gewillig MH, et al. Evaluation and management of the child and adult with Fontan circulation: a scientific statement from the American Heart Association. *Circulation*. 2019;140:e234-84.
2. Douglas WI, Goldberg CS, Mosca RS, Law IH, Bove EL. Hemi-Fontan procedure for hypoplastic left heart syndrome: outcome and suitability for Fontan. *Ann Thorac Surg*. 1999;68:1361-7; discussion 1368.
3. Spray TL. Hemi-Fontan procedure. *Oper Tech Thorac Cardiovasc Surg*. 2013;18:124-37.
4. Rijnberg FM, Hazekamp MG, Wentzel JJ, de Koning PJH, Westenberg JJM, Jongbloed MRM, et al. Energetics of blood flow in cardiovascular disease: concept and clinical implications of adverse energetics in patients with a Fontan circulation. *Circulation*. 2018;137:2393-407.
5. McLennan D, Schäfer M, Mitchell MB, Morgan GJ, Ivy D, Barker AJ, et al. Usefulness of 4D-flow MRI in mapping flow distribution through failing Fontan circulation prior to cardiac intervention. *Pediatr Cardiol*. 2019;40:1093-6.
6. Bove EL, de Leval MR, Migliavacca F, Guadagni G, Dubini G. Computational fluid dynamics in the evaluation of hemodynamic performance of cavopulmonary connections after the Norwood procedure for hypoplastic left heart syndrome. *J Thorac Cardiovasc Surg*. 2003;126:1040-7.
7. Kung E, Corsini C, Marsden A, Vignon-Clementel I, Pennati G, Figliola R, et al. Multiscale modeling of superior cavopulmonary circulation: hemi-Fontan and bidirectional Glenn are equivalent. *Semin Thorac Cardiovasc Surg*. 2020;32:883-92.
8. Pekkan K, Dasi LP, De Zélicourt D, Sundareswaran KS, Fogel MA, Kanter KR, et al. Hemodynamic performance of stage-2 univentricular reconstruction: Glenn vs. hemi-Fontan templates. *Ann Biomed Eng*. 2009;37:50-63.
9. Dyverfeldt P, Bissell M, Barker AJ, Bolger AF, Carlhäll CJ, Ebbers T, et al. 4D flow cardiovascular magnetic resonance consensus statement. *J Cardiovasc Magn Reson*. 2015;17:72.
10. Cibis M, Jarvis K, Markl M, Rose M, Rigsby C, Barker AJ, et al. The effect of resolution on viscous dissipation measured with 4D flow MRI in patients with Fontan circulation: evaluation using computational fluid dynamics. *J Biomech*. 2015;48:2984-9.
11. Rijnberg FM, Westenberg JJM, van Assen HC, Juffermans JF, Kroft LJM, van den Boogaard PJ, et al. 4D flow cardiovascular magnetic resonance derived energetics in the Fontan circulation correlate with exercise capacity and CMR-derived liver fibrosis/congestion. *J Cardiovasc Magn Reson*. 2022;24:21.
12. Lee GH, Koo HJ, Park KJ, Yang DH, Ha H. Characterization of baseline hemodynamics after the Fontan procedure: a retrospective cohort study on the comparison of 4D flow MRI and computational fluid dynamics. *Front Physiol*. 2023;14:1199771.
13. Barker AJ, van Ooij P, Bandi K, Garcia J, Mazen Albaghdadi M, McCarthy P, et al. Viscous energy loss in the presence of abnormal aortic flow. *Magn Reson Med*. 2014;72:620-8.
14. Schäfer M, Di Maria MV, Jaggers J, Stone ML, Ivy DD, Barker AJ, et al. High-degree Norwood neoaortic tapering is associated with abnormal flow conduction and elevated flow-mediated energy loss. *J Thorac Cardiovasc Surg*. 2021;162:1791-804.
15. Stone ML, Schäfer M, DiMaria MV, von Alvensleben JC, Campbell DN, Jaggers J, et al. Diastolic inflow is associated with inefficient ventricular flow dynamics in Fontan patients. *J Thorac Cardiovasc Surg*. 2022;163:1195-207.
16. Schäfer M, Ivy DD, Abman SH, Stenmark K, Browne LP, Barker AJ, et al. Differences in pulmonary arterial flow hemodynamics between children and adults with pulmonary arterial hypertension as assessed by 4D-flow CMR studies. *Am J Physiol Circ Physiol*. 2019;316:H1091-104.
17. Ho J, Tumkaya T, Aryal S, Choi H, Claridge-Chang A. Moving beyond P values: data analysis with estimation graphics. *Nat Methods*. 2019;16:565-6.
18. Bove EL, de Leval MR, Migliavacca F, Balossino R, Dubini G. Toward optimal hemodynamics: computer modeling of the Fontan circuit. *Pediatr Cardiol*. 2007;28:477-81.
19. Kung E, Baretta A, Baker C, Arbia G, Biglino G, Corsini C, et al. Predictive modeling of the virtual hemi-Fontan operation for second stage single ventricle palliation: two patient-specific cases. *J Biomech*. 2013;46:423-9.
20. Guadagni G, Bove EL, Migliavacca F, Dubini G. Effects of pulmonary afterload on the hemodynamics after the hemi-Fontan procedure. *Med Eng Phys*. 2001;23:293-8.
21. Sun Q, Wan D, Liu J, Hong H, Liu Y, Zhu M. Patient-specific computational fluid dynamic simulation of a bilateral bidirectional Glenn connection. *Med Biol Eng Comput*. 2008;46:1153-9.
22. Cheng AL, Wee CP, Pahlevan NM, Wood JC. A 4D flow MRI evaluation of the impact of shear-dependent fluid viscosity on in vitro Fontan circulation flow. *Am J Physiol Heart Circ Physiol*. 2019;317:H1243-52.
23. Rijnberg FM, Elbaz MSM, Westenberg JJM, Kamphuis VP, Helbing WA, Kroft LJ, et al. Four-dimensional flow magnetic resonance imaging-derived blood flow energetics of the inferior vena cava-to-extracardiac conduit junction in Fontan patients. *Eur J Cardiothoracic Surg*. 2019;55:1202-10.
24. Kamphuis VP, Westenberg JJM, van der Palen RLF, van den Boogaard PJ, van der Geest RJ, de Roos A, et al. Scan-rescan reproducibility of diastolic left ventricular kinetic energy, viscous energy loss and vorticity assessment using 4D flow MRI: analysis in healthy subjects. *Int J Cardiovasc Imaging*. 2018;34:905-20.

25. Schäfer M, Barker AJ, Kheyfets V, Stenmark KR, Crapo J, Yeager ME, et al. Helicity and vorticity of pulmonary arterial flow in patients with pulmonary hypertension: quantitative analysis of flow formations. *J Am Heart Assoc*. 2017; 6:e007010.
26. Oganesyan A, Hoffner-Heinike A, Barker AJ, Frank BS, Ivy DD, Hunter KS, et al. Abnormal pulmonary flow is associated with impaired right ventricular coupling in patients with COPD. *Int J Cardiovasc Imaging*. 2021;37:3039-48.

Key Words: hemi-Fontan, bidirectional Glenn, flow hemodynamics